- Supporting Information -

Stout Fluorescence Enhancement of Fungicide Thiabendazole by Van der Walls Interaction with Transition Metal Dichalcogenide Nanosheets for Highly Specific Sensors

*Elías Blanco, José I. Martínez, Ana María Parra-Alfambra, María Dolores Petit-Domínguez, María del Pozo, José A. Martín-Gago, Elena Casero, Carmen Quintana**

S1. Influence of the Nanomaterials and Solvent Amount Employed to TMDs Exfoliation on the Fungicide Fluorescence.

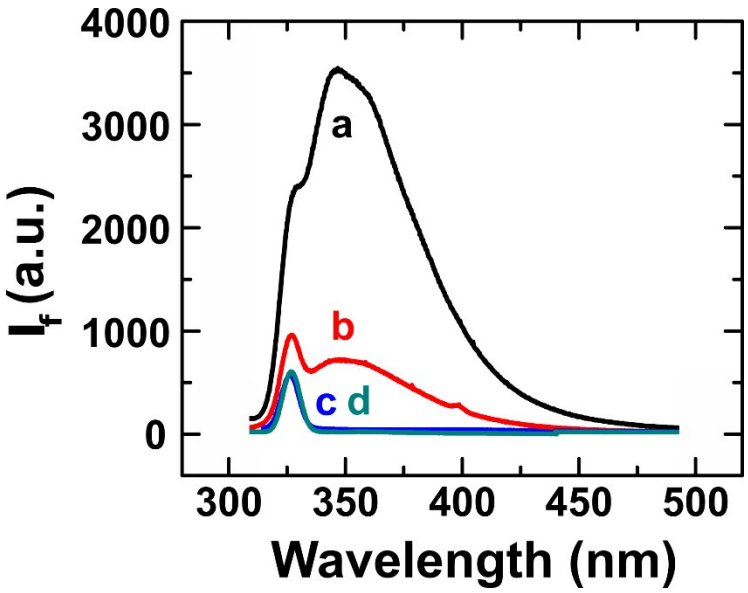

Figure S1. Fluorescence spectra of a) 100 nM TBZ + 200 µL of WS_2 exfoliated in EtOH/H_2O; b) 100 nM TBZ + 200 µL of exfoliation solvent; c) 200 µL of WS_2 exfoliated in EtOH/H_2O and d) exfoliation solvent.

Figure S1 shows the fluorescence spectra of solutions containing mixtures of the fluorophore TBZ and the nanomaterial (WS_2) prepared using EtOH/H_2O as exfoliation solvent, together with the spectra of the different reagents employed. As observed, neither the 2D nanomaterial nor the exfoliation solvent employed (curves c and d, respectively) contribute with additional signal to the increase of fluorescence measured at 350 nm when TBZ interacts with the TMD (curve a respect to curve b).

Scheme S1 displays the molecular structures of the fungicides studied.

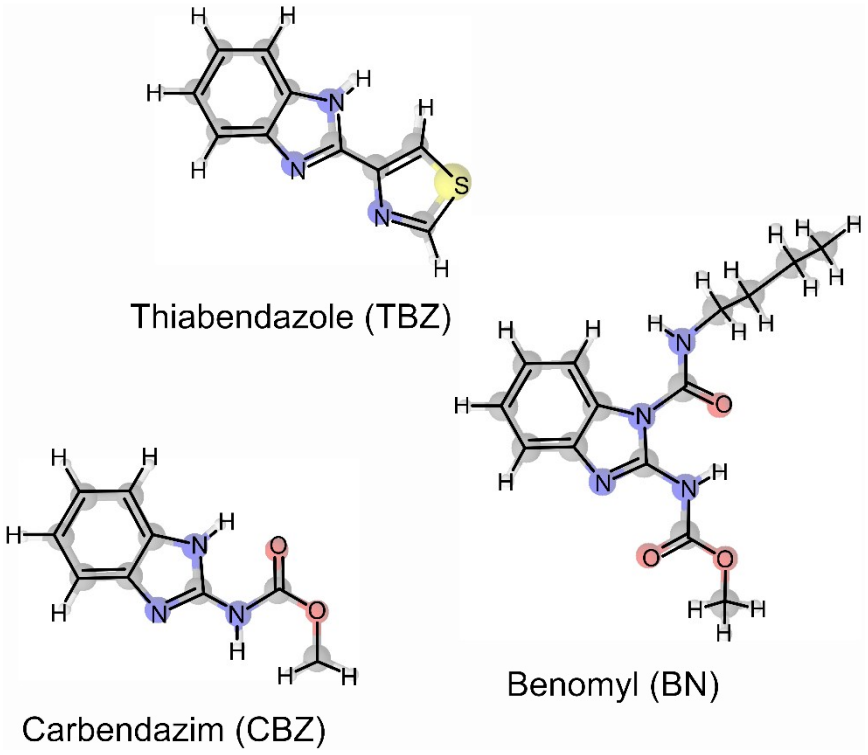

Scheme S1. Molecular structures of fungicides.

S2. Description of the Different DFT-optimized (CBZ/TBZ)/MoS_2, (CBZ/TBZ)/Gr, and (CBZ/TBZ)/GOx Interfacial Configurations

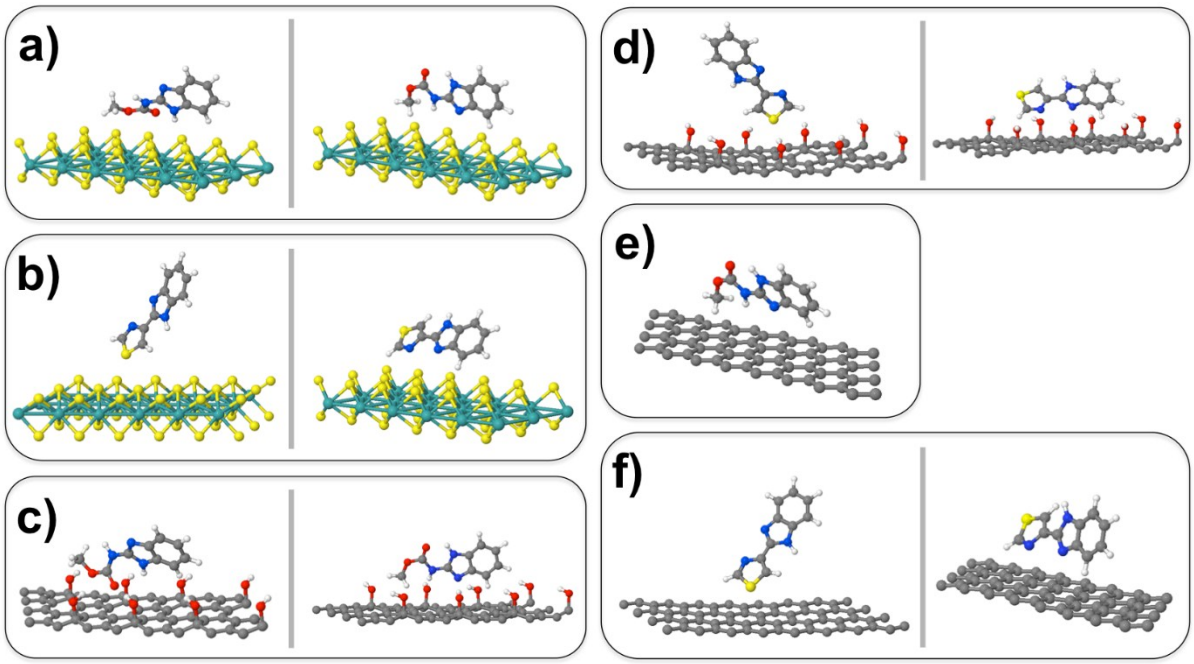

Figure S2. Pictorial view of the DFT-based optimized interfacial systems: a) CBZ/MoS_2, b) TBZ/MoS_2, c) CBZ/GOx, d) TBZ/GOx, e) CBZ/Gr, and f) TBZ/Gr. Among all the interfacial configurations analysed, each panel shows the most stable configurations lying within a total energy range < 0.2 eV.

Figure S2 shows the most stable configurations for the interfaces formed between the CBZ and TBZ molecules and the single layer MoS_2, Gr and GOx substrates (for each system the figure shows those configurations lying within a total energy range < 0.2 eV). Within all the interfacial systems analysed, the character of the molecule/substrate interaction is mainly driven by electrostatic and van der Waals forces, exhibiting an almost negligible chemical

interaction. Nonetheless, in most cases, this interaction is strong enough to anchor the molecules to the surface, even to slightly disrupt the gas-phase molecular geometries. This behaviour could be a priori expected, given the chemical inertness nature of the substrates. Starting with the CBZ/MoS_2 interface (Figure S2a) the preferential molecular adsorption configurations show, in one case, the molecule interacting with the substrate via the $-COOCH_3$ ester group, leaving the rest of the molecule slightly twisted away (left). Whilst in the other configuration (right) the molecule tends to maximize the interaction with the substrate via the non-hydrogenated N atom of the molecular pentagon and the terminating $-CH_3$ group of the ester. These two configurations, for which no molecular distortion is observed (see Figure S3a), yield molecular binding energies (E_b) of 0.95 and 1.10 eV, respectively.

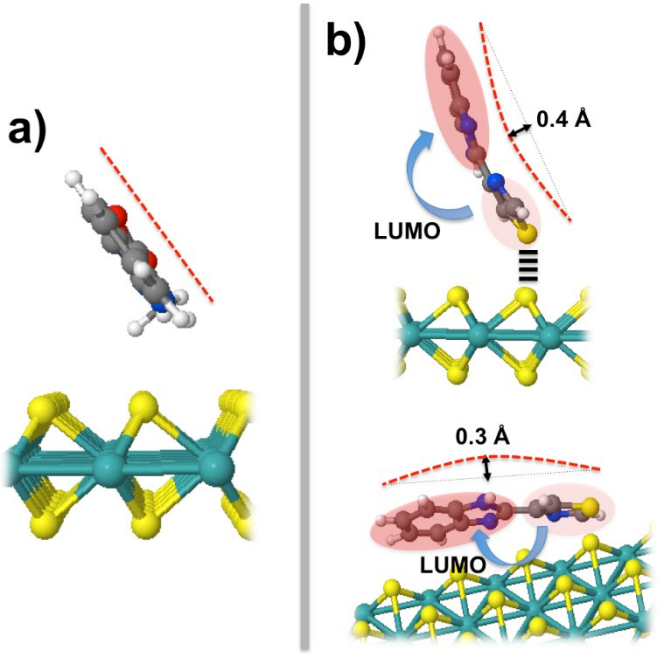

Figure S3. Pictorial view of the on-surface molecular distortions experienced by the CBZ and TBZ molecules on the MoS_2 monolayer. (a) No significant molecular distortion is observed for the most stable CBZ/MoS_2 interfacial configuration. (b) A pronounced molecular bending is observed for the two most stable isoenergetic TBZ/MoS_2 interfacial configurations.

For the TBZ/MoS_2 case one of the preferential molecular adsorption configurations (Figure S2b left) shows the molecule interacting with the substrate via its terminating S-atom (at an adsorption perpendicular distance w.r.t. the average topmost S-plane of around 2.2 Å), yielding a binding energy of around 1.15 eV. This particular substrate/adsorbate interaction induces a net molecular distortion characterized by a bending after deposition of around 0.4 Å (see Fig. S3b, top), which will have a clear reflection on its electronic and excitation properties. In the other configuration (Figure S2b, right) the molecule again tends to maximize the interaction with the substrate via the non-hydrogenated N atom of the molecular pentagon with a very close binding energy value w.r.t. the previous configuration (~1.18 eV) and a slightly bent (0.3 Å) molecular geometry (see Fig. S3b, bottom). We have checked that the possibility of presence of S-vacancies in the substrate does not importantly alter these results (see Fig. S4).

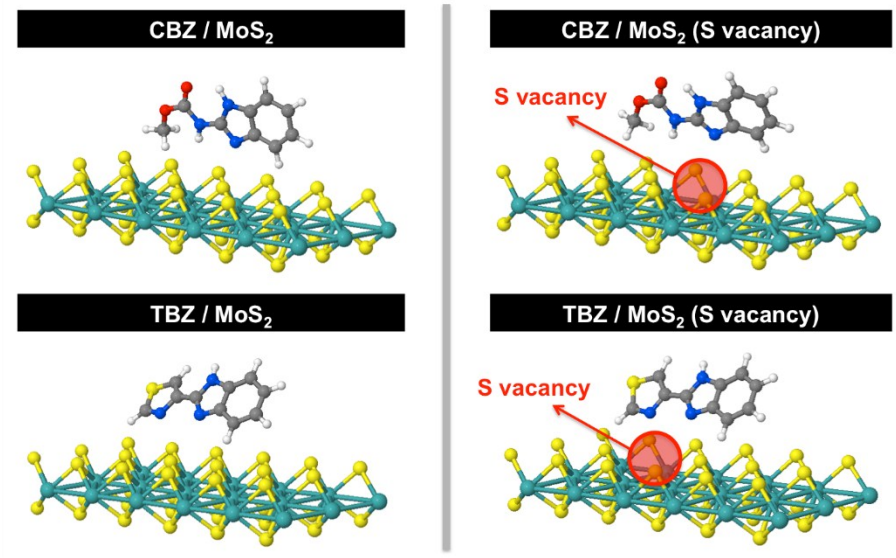

Figure S4. Pictorial comparative view of the DFT-based optimized interfacial systems: (left) CBZ/MoS_2 and TBZ/MoS_2, and (right) CBZ/MoS_2(S vacancy) and TBZ/MoS_2(S vacancy). No significant structural differences are observed between the interfaces with unaltered MoS_2 and the defective MoS_2(S vacancy).

The most stable configurations for the (CBZ/TBZ)/Gr cases (Figures S2e,f) can be grouped within the same interaction category, yielding weaker adsorption energies than in the previous cases ranging between 0.5 and 0.65 eV. Finally, the (CBZ/TBZ)/GOx interfaces (Figures S2c, d) yield the stronger molecular adsorption energies ranging between 1.20 and 1.35 eV. The adsorption configurations in these cases tend to stabilize the molecule/substrate interaction by the creation of dipolar bonds between the –OH groups of the substrate and the O and N atoms of the CBZ, and the S and N atoms of the TBZ molecules. The strength of the dipolar interaction is evident regarding the on-surface orientation of the OH groups to maximize the dipolar coupling.

S3. Density of Electronic States for the Free CBZ and TBZ Molecules, and for the Optimized (CBZ/TBZ)/MoS_2, (CBZ/TBZ)/Gr, and (CBZ/TBZ)/GOx Interfacial Configurations

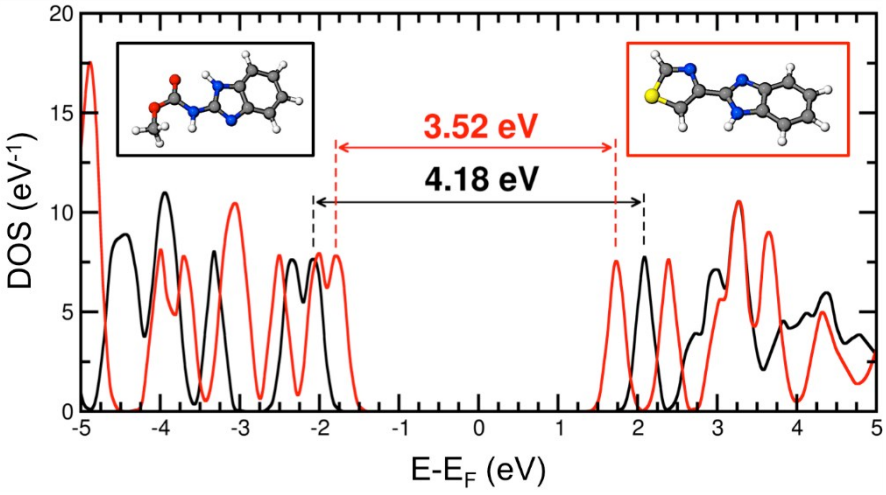

Figure S5. Computed density of electronic states (in eV^{-1}) as a function of the energy (in eV), referred to the Fermi energy, for the free CBZ (black line) and TBZ (red line) molecules. Molecular transport gaps for both molecules are also indicated.

Figure S5 shows the computed density of electronic states as a function of the energy, referred to the Fermi energy, for the free CBZ and TBZ molecules. Conventional DFT yields molecular transport gaps of 4.18 and 3.52 eV for the free CBZ and TBZ molecules, respectively. This difference between both molecular gaps could explain the different wavelength for the most important optical absorption and emission peaks in both molecules. Additionally, in order to check the influence in the molecular electronic properties after the different (CBZ/TBZ)/MoS_2, (CBZ/TBZ)/GOx and (CBZ/TBZ)/Gr interfaces are formed we have also computed the density of electronic states projected onto the CBZ (Figure S6) and TBZ (Figure S7) molecules within the different interfaces. Results of these simulations reveal that the molecular gaps are reduced after the different interfaces are formed, from 4.18 up to 3.14 eV for the CBZ, and from 3.52 up to 2.51 eV for the TBZ depending on the specific interfacial configuration. Interestingly, no significant morphological changes are observed in the DOS profiles between the free and adsorbed on-surface forms, which indicate the strong electrostatic nature of all the interfacial interactions. On the other side, the gap-closing effect observed in most cases may be attributed to the on-surface geometrical distortions of different degrees, as well as spreading out of the HOMO and LUMO states by effect of the interfacial interaction.

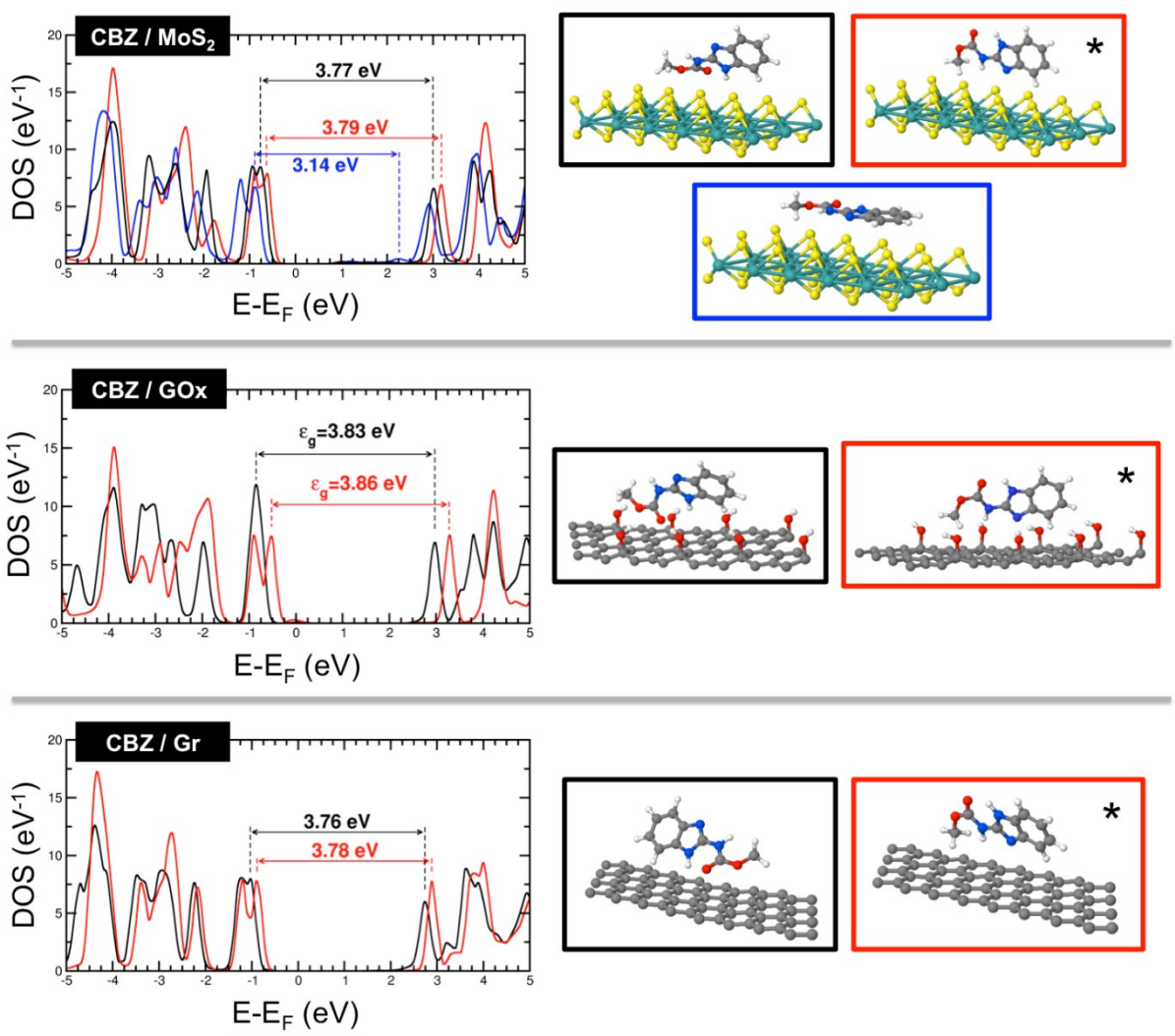

Figure S6. Computed density of electronic states (in eV^{-1}) as a function of the energy (in eV), referred to the Fermi energy, projected onto the CBZ molecules forming the CBZ/MoS_2 (top panel), CBZ/GOx (middle panel) and CBZ/Gr (bottom panel) interfaces. Molecular transport gaps are also indicated. Pictorial view of the DFT-based optimized interfacial systems are shown with a coloured frame corresponding to the associated DOS profile colour line. The most stable interfacial configurations are indicated by an "*". Notice that for the CBZ/MoS_2 interface (top panel), an additional optimized configuration w.r.t. the Figure S2 (blue framed), less stable energetically than the other two structures, is shown for comparative purposes.

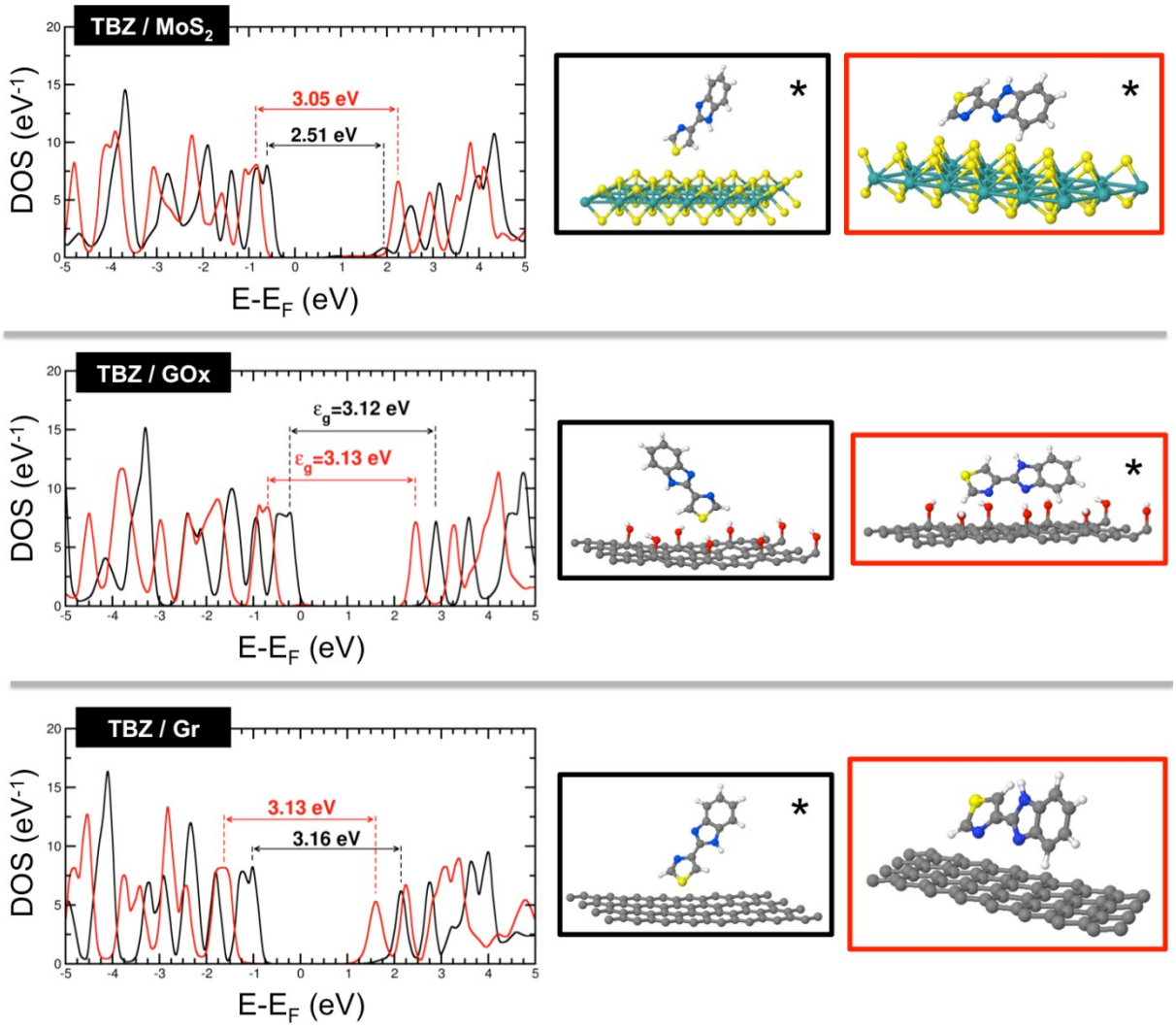

Figure S7. Computed density of electronic states (in eV^{-1}) as a function of the energy (in eV), referred to the Fermi energy, projected onto the TBZ molecules forming the TBZ/MoS_2 (top panel), TBZ/GOx (middle panel) and TBZ/Gr (bottom panel) interfaces. Molecular transport gaps are also indicated. Pictorial view of the DFT-based optimized interfacial systems are shown with a coloured frame corresponding to the associated DOS profile colour line. The most stable interfacial configurations are indicated by an "*", except for the TBZ/MoS_2 case (top panel), where both configurations are isoenergetic.

S4. Different Methods for Determination of TBZ and Detection Limits

Table S1. Methods for determination of TBZ in the literature indicating the linear range and the detection limit (LOD). EQ: electrochemical technique. LC: liquid chromatography. CE: capillary electrophoresis. RTP: room-temperature phosphorescence. FL: fluorescence. CL: chemiluminiscence.

Method	Linear range (nM)	LOD (nM)	Reference
EQ	5×10^2-10^5	50	[23]
LC	250-9×10^4	22	[39]
LC	50-10^4	25	[40]
RTP	76-745	76	[41]
RTP	99-41×10^2	10	[42]
CE	10^3-25×10^3	164	[43]
CE	18-25×10^2	5	[44]
FL	250-5×10^3	36	[45]
FL	4×10^2-5×10^3	56	[46]
FL	0-5×10^4	18	[22]
CL	5-1×10^4	1.5	[47]
FL	5-250	2.7	This work

S5. DFT-based Calculation of the C—C Bond Rigidity Linking the Aromatic Subunits in TBZ in its Free and On-surface Adsorbed Forms

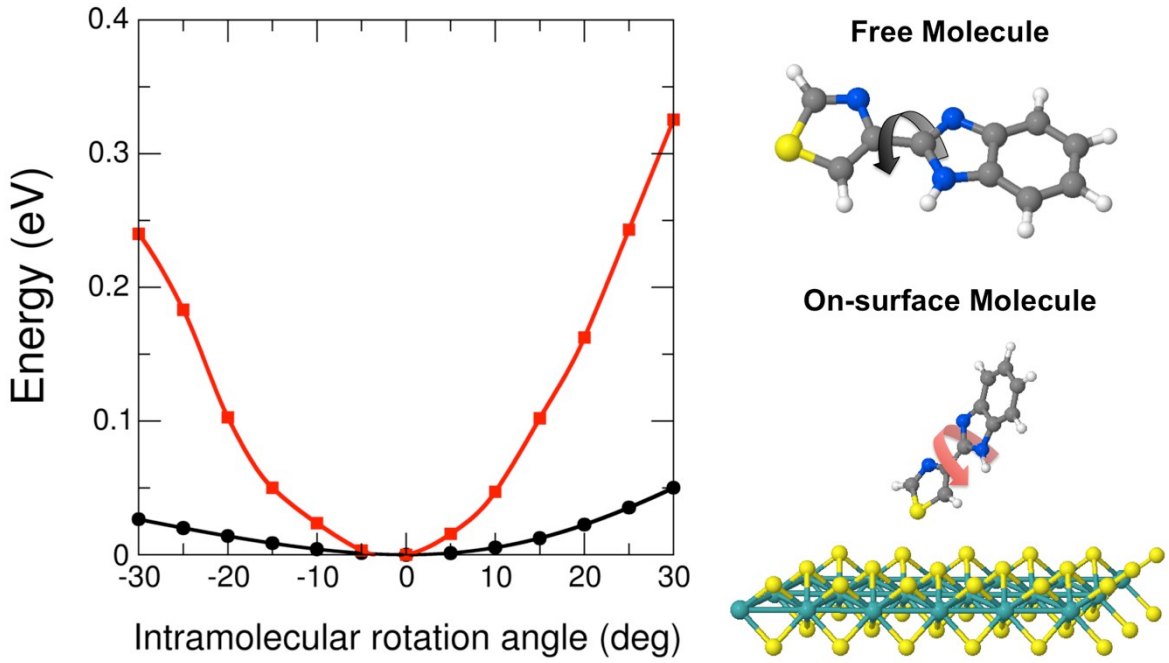

Figure S8. Computed energy (in eV) as a function of the intramolecular rotation angle (in degrees) of the C—C bond linking the aromatic subunits in TBZ between -30º and 30º around the longitudinal molecular axis for both its optimized free (black line) and on-surface adsorbed (red line) forms. Energy is referred to the minimum energy values at 0º (considered as the angle in its ground-state free and on-surface adsorbed forms). Surface is MoS_2.

Figure S8 shows the computed energy (in eV) as a function of the intramolecular rotation angle (in degrees) of the C—C bond linking the aromatic subunits in TBZ between -30º and 30º around the longitudinal molecular axis for both its optimized free (black line) and on-surface adsorbed (red line) forms. As one can notice from the figure, intramolecular rotation for the TBZ in its free form occurs easily, yielding potential energies between 0.025 and 0.5 eV. These low values indicate that the rotation of the molecule in gas phase or dissolution

takes place continuously at room temperature. Nonetheless, once adsorbed on the MoS_2 surface, the intramolecular rotation results hindered by the stiffness of the C—C bond, yielding values of around one order of magnitude higher.